

Concentration of Measure for Distributions Generated via Diffusion Models

Reza Ghane ^{*†} Anthony Bao ^{*‡} Danil Akhiamov ^{*§} Babak Hassibi ^{†§}

January 15, 2025

Abstract

We show via a combination of mathematical arguments and empirical evidence that data distributions sampled from diffusion models satisfy a Concentration of Measure Property saying that any Lipschitz 1-dimensional projection of a random vector is not too far from its mean with high probability. This implies that such models are quite restrictive and gives an explanation for a fact previously observed in Pandey et al. [2024] that conventional diffusion models cannot capture "heavy-tailed" data (i.e. data \mathbf{x} for which the norm $\|\mathbf{x}\|_2$ does not possess a subgaussian tail) well. We then proceed to train a generalized linear model using stochastic gradient descent (SGD) on the diffusion-generated data for a multiclass classification task and observe empirically that a Gaussian universality result holds for the test error. In other words, the test error depends only on the first and second order statistics of the diffusion-generated data in the linear setting. Results of such forms are desirable because they allow one to assume the data itself is Gaussian for analyzing performance of the trained classifier. Finally, we note that current approaches to proving universality do not apply to this case as the covariance matrices of the data tend to have vanishing minimum singular values for the diffusion-generated data, while the current proofs assume that this is not the case (see Subsection 3.4 for more details). This leaves extending previous mathematical universality results as an intriguing open question.

1 Introduction

One of the most astonishing contributions of deep learning is the advent of generative models for image and video generation. Diffusion-based generative models Sohl-Dickstein et al. [2015], Song and Ermon [2019], Ho et al. [2020], Song et al. [2020], Dhariwal and Nichol [2021], Song et al. [2021], Kingma et al. [2021], Karras et al. [2022], in particular, have enjoyed tremendous success in vision [LDM Rombach et al. [2022], audio [Diffwave Kong et al. [2020]] and text generation [D3PM Austin et al. [2021]]. For an overview of diffusion models and their applications, we refer to the surveys Croitoru et al. [2023] and Yang et al. [2023].

Despite significant progress in training methods, network architecture design, and hyperparameter tuning, there has been relatively little work done on understanding rigorous mathematical properties of the data generated by diffusion models. Through theory and experiments, we argue that

*Equal Contribution

[†]Department of Electrical Engineering, California Institute of Technology

[‡]Department of Electrical and Computer Engineering, University of Texas at Austin

[§]Department of Computing and Mathematical Sciences, California Institute of Technology

images generated by conventional diffusion models are mathematically tractable. In fact, we argue that when the reverse process is a contraction, one could establish a concentration of measure phenomenon for the distribution of the output. Since the latter hints that some sort of Gaussian Universality might hold, we compare the generalization error of linear models trained on diffusion data to the the generalization error of linear models trained on Gaussian Mixtures with matching means and covariances and observe a close match.

While there are many aspects to building a diffusion model for data synthesis such as training the denoiser, choice of the forward process and the scheduler, in this work we take a higher level approach and mainly focus on the sampling process of a pre-trained diffusion model and our arguments are agnostic to the training procedure and the denoiser’s architecture details.

We believe that the present study is important both for advancing our theoretical understanding of generative models for images and their limitations, as well as the role of data in supervised ML:

- We show that distributions that can be generated via diffusion models are far from arbitrary and share many properties with Gaussian distributions in a precise mathematical sense. In particular, this implies the empirical observation made in Pandey et al. [2024] that the traditional diffusion models are bad for generating distributions with heavy tails, but this could be remedied by passing a heavy-tailed noise from the beginning.
- As discussed in Goldblum et al. [2023] and Nakkiran [2021], one of the major factors that hinders us from having a solid theory of deep learning is the lack of practical assumptions amenable to clean mathematical formulations and analyses regarding the true distributions of data. We believe that our work sheds light on this question in the context of image classification tasks. To elaborate further on this point, note that most image data sets encountered in practice *can* be approximated well using data sampled from diffusion models. This suggests that in a sense it is enough to explain generalization for data coming from GMMs. The latter has been a topic of active research recently; see, e.g. Thrampoulidis et al. [2020], Loureiro et al. [2021b].

2 Related Works

The theoretical analysis of diffusion models and the images generated by such models remains an underexplored area of work.

- By focusing on Langevin dynamics, in an emerging line of work, many papers have analyzed the output distributions of the diffusion models and the convergence of the diffusion models. Chen et al. [2022] have shown that in DDPM and CLD, one can arbitrarily obtain a close approximation of any distribution, assuming the ability of the diffusion model to capture the distribution and this assumption is central to most of works done in this area. In fact, this work is among the first to provide quantitative polynomial bounds, capturing the high-dimensionality of the data. Unfortunately, in practice, given the high-dimensional nature of the problem, estimating the score function might be impossible. Furthermore, in practice it is unfeasible to verify the validity of this assumption in particular as we do not have access to the true score function. On the other hand, evident by the bounds of Mousavi-Hosseini et al. [2023], in general generating heavy tailed distributions using Langevin Dynamics from Gaussians is intractable in practice as one need to run the Langevin dynamics for exponential number of steps. We refer to Li et al. [2024a] for a brief overview of works done on the

convergence theory of diffusion models.

- Seddik et al. [2020] showed a form of equivalence between representations generated from Generative Adversarial Networks and from the Gaussian Mixture Models. The authors considered the Gram matrix of pre-trained classifier representations of the GAN-generated images and showed that asymptotically, it has the same distribution of eigenvalues as the Gram matrix of Gaussian samples with matching first and second moments.
- In the context of classification of Gaussian mixture models, Loureiro et al. [2021b] investigated the validity of their results for the asymptotics of linear models for binary classification with logistic loss and ℓ_2 regularization. They tested their findings on MNIST and Fashion MNIST datasets where they observed close match in the generalization error for the real images and their corresponding Gaussian mixture model. Furthermore, they go beyond linear models and observe a similar behavior in a feature map obtained by training a two-layer neural network. Loureiro et al. [2021a] considered Student-teacher model and verified universality for MNIST and Fashion MNIST via kernel ridge regression. They also explored dcGAN-generated data, labeling it using a three-layer teacher network. Using logistic regression for classification illustrated a close match with GMMs on GAN-generated data, but deviation in real-world samples from CIFAR10 was observed. Then Pesce et al. [2023] analyzed the student-teacher model for classification and empirically demonstrated the universality of double descent for MNIST and fashion MNIST datasets. These datasets were processed using a random feature map, with labels generated by a random teacher, for both ridge regression and logistic classification tasks. However, they also present that the universality of the test error fails to hold while using the data from CIFAR-10 without any preprocessing or using wavelet scattering or Hadamard orthogonal projection to preprocess the data. And Dandi et al. [2024] observe empirically that the data distributions generated by conditional GANs (cGANs) pretrained on fashion-MNIST dataset exhibit Gaussian universality of the test error of generalized linear models. The universality part of our work can be considered as an exploration of the same phenomenon for conditional diffusion models trained on significantly larger image datasets. Gerace et al. [2024] considering mixture distributions with random labels, they demonstrated universality of test of the generalized linear models on real-world datasets such as MNIST, CIFAR10 with GMMs.
- Refinetti et al. [2023] showcase that SGD learns higher moments of the data as the training continues. Moreover, they show that in the case of training more sophisticated nonlinear models on the data, such as Resnet18, universality of the test error breaks when one replaces the input data by its corresponding gaussian mixture or data generated by WGANs. Exploring the limitations of current universality results and conditions under which they break remains an interesting direction of research.
- Jacot et al. [2020] and Bordelon et al. [2020] considered Kernel methods for regression and corroborated their findings by experiments over the over MNIST and Higgs datasets and providing evidence of gaussian universality.
- Pandey et al. [2024] explore heavy-tailed data generation using diffusion models. They also observe that this is not possible if one passes Gaussian noise to the models as it is usually done and suggest using Student t-distribution instead. Pandey et al. [2024] then demonstrate numerically that their scheme works well in practice for generating the HRRR dataset Dowell et al. [2022].
- Li et al. [2024b] explore a connection between diffusion models and the GMMs constructed from data from a different point of view. Namely, they observe that if the denoisers are over-parametrized the diffusion models arrive at the Gaussian Mixture Models with the means and covariances matching those of the training dataset but learn to diverge from at later stages of

training. Our observations imply that even though the distribution of the diffusion-generated images stops being the same as the corresponding GMM after sufficiently many training steps, they still have many properties in common.

3 Preliminaries and the theory

We start by defining a key notion needed for our results and then move on to provide an overview of the sampling process of diffusion models. We also prove a universality result for linear models in multiclass classification tasks. We conclude this section by stating our main findings.

3.1 Concentration of Measure Property

We use the following definition of concentration. Informally, it means that the tails of the distribution decay exponentially fast. Note that it corresponds to the Lipschitz Concentration Property for $q = 2$ from Seddik et al. [2020].

Definition 1 (CoM). *Given a probability distribution $x \sim \mathbb{P}$ where $\mathbf{x} \in \mathbb{R}^d$, we say that \mathbf{x} satisfies the Concentration of Measure Property (CoM) if there exist $C, \sigma > 0$ such that for any L -Lipschitz function $f : \mathbb{R}^d \rightarrow \mathbb{R}$ it holds that*

$$\mathbb{P}(|f(\mathbf{x}) - \mathbb{E}f(\mathbf{x})| > t) \leq Ce^{-(\frac{t}{L\sigma})^2} \quad (1)$$

The distributions satisfying CoM arise naturally in many applications and are quite ubiquitous. We appeal to the following proposition proven in Rudelson and Vershynin [2013] :

Proposition 1. *The distribution $\mathbf{x} \sim \mathcal{N}(0, \Sigma)$ satisfies the CoM property 1. Moreover, the corresponding $C = 2$ and $\sigma = \|\Sigma^{\frac{1}{2}}\|_{op}$.*

If $\Sigma = \frac{\mathbf{I}_d}{d}$ and $f(\mathbf{x}) = \|\mathbf{x}\|_2$, then Proposition 1 implies the classical fact that the norm of the normalized standard vector converges to 1 in probability as $d \rightarrow \infty$ because in this case the upper bound of Definition 1 becomes $2e^{-(\frac{t}{\sigma})^2} = 2e^{-td} \rightarrow 0$. However, if Σ is also normalized as $\text{Tr}(\Sigma) = 1$ but $\|\Sigma\|_{op} = \Theta(1)$ (which happens, for example, if the ordered eigenvalues of Σ follow the power law $\lambda_i = Ci^{-\alpha}$ for some $C > 0$ and $\alpha > 1$), then the variance of \mathbf{x} does not have to go to zero anymore, but Definition 1 still implies that \mathbf{x} has exponentially decaying tails (to be more precise, \mathbf{x} is a sub-Gaussian random vector—see Definition 3.4.1 in Vershynin [2018]) and in particular cannot be heavy-tailed. The latter was empirically demonstrated via an extensive set of experiments in Pandey et al. [2024] and therefore our results can be considered to be a theoretical validation of the corresponding body of simulations presented in Pandey et al. [2024].

Gaussians are far from the only distributions satisfying CoM; other examples include the strongly log-concave distributions, the Haar measure and we refer to Section 5.2 in Vershynin [2018] for more examples. The concentration of measure phenomenon has played a key role in the development of many areas such as random functional analysis, compressed sensing, and information theory.

3.2 Diffusion

We provide an overview of diffusion models pertinent to our results in this paper. Given samples $x_0 \sim q_0$ from a high-dimensional distribution in \mathbb{R}^n , we learn a distribution $p_\theta \approx q_0$ that allows

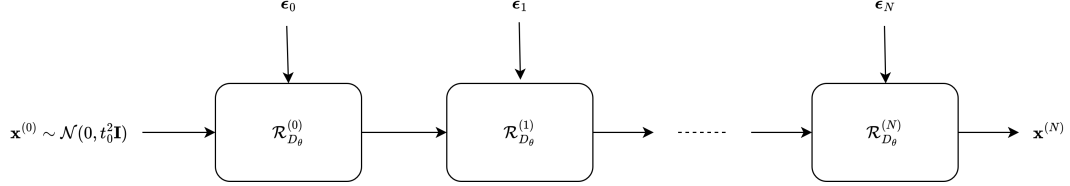


Figure 1: High level overview of the sampling process in the diffusion models

easy sampling. A trained diffusion model essentially applies a sequence of nonlinear mappings (specifically, denoisers, denoted by D_θ) to a white Gaussian input to obtain clean images. Following the formulation in Karras et al. [2022], assuming the distribution of the training to be "delta dirac", the score function can be expressed in terms of the ideal denoiser that minimizes L_2 error for every noise scale, i.e. $\nabla_{\mathbf{x}} \log p(\mathbf{x}; \sigma) = (D_\theta(\mathbf{x}; \sigma) - \mathbf{x})/\sigma^2$. This serves as a heuristic for using $(D_\theta(\mathbf{x}; \sigma) - \mathbf{x})/\sigma^2$ as a surrogate for the score function to run the backward process. In most applications, D_θ is a neural network trained to be a denoiser, typically using a U-Net backbone. The specific denoiser we consider for our experiments is from ADM Dhariwal and Nichol [2021] which uses a modified U-Net backbone with self-attention layers. During training, the network sees multiple noise levels, and so learns to denoise at many scales. Our analysis and statements in Section 3.5 hold for most of the diffusion models used in practice, as they employ a Lipschitz neural network. In the view of the discussion above, and setting $\sigma(t) = t$, we can represent the sampling process as an iterative procedure of N steps, expressed as:

$$\mathbf{x}_0 \approx \mathbf{x}^{(N)} = \mathcal{R}_{D_\theta}^{(N-1)}(\mathcal{R}_{D_\theta}^{(N-2)}(\dots \mathcal{R}_{D_\theta}^{(0)}(\mathbf{x}^{(0)}, t_{0:1}) \dots), t_{N-2:N-1}), t_{N-1:N}) \quad (2)$$

Where $\mathbf{x}_T := \mathbf{x}^{(0)} \sim \mathcal{N}(0, t_0^2 \mathbf{I})$ is isotropic Gaussian noise and $\mathbf{x}_0 \approx \mathbf{x}^{(N)}$ is the clean image. We adopt this notation of sub-scripting the time index for \mathbf{x} while super-scripting its sampler step index in order to avoid confusion with the standard notation in diffusion model papers. At any sampler step i we have a (noisy image, noise level) pair $(\mathbf{x}^{(i)}, t_i)$ and the next noise level t_{i+1} ; and $\mathcal{R}_{D_\theta}^{(i)}$ represents the mapping used to generate a less noisy sample i.e. $\mathbf{x}^{(i+1)} \leftarrow \mathcal{R}_{D_\theta}^{(i)}(\mathbf{x}^{(i)}, t_{i:i+1})$, which takes in an independent noise ϵ_i at each time step, as illustrated by Figure 1.

Algorithm 1: EDM Stochastic Sampler Karras et al. [2022]

```

1 Define  $f(\mathbf{x}, t) := (\mathbf{x} - D_\theta(\mathbf{x}, t)) / t$ ; • Simplified Probability Flow ODE
2 Sample  $\mathbf{x}^{(0)} \sim \mathcal{N}(0, t_0^2 \mathbf{I})$ 
3 for  $i \in \{0, \dots, N-1\}$  do
4   Sample  $\epsilon \sim \mathcal{N}(0, S_{\text{noise}}^2 \mathbf{I})$ 
5    $\hat{\mathbf{x}}^{(i)} \leftarrow \mathbf{x}^{(i)} + t_i \sqrt{\gamma(2+\gamma)} \epsilon$ ; • Inject Additional Noise
6    $h \leftarrow t_{i+1} - t_i(1+\gamma)$ ; • Step size
7    $\mathbf{x}^{(i+1)} \leftarrow \hat{\mathbf{x}}^{(i)} + hf(\hat{\mathbf{x}}^{(i)}, t_i(1+\gamma))$ ; • Euler step
8   if  $t_{i+1} \neq 0$  then
9      $\mathbf{x}^{(i+1)} \leftarrow \hat{\mathbf{x}}^{(i)} + \frac{h}{2} (f(\hat{\mathbf{x}}^{(i)}, t_i(1+\gamma)) + f(\mathbf{x}^{(i+1)}, t_{i+1}))$ ; • Second-order correction
10 return  $\mathbf{x}^{(N)}$ 

```

In this work, we focus on the framework considered in Karras et al. [2022] and we observe that in

summary, $\mathbf{x}^{(i+1)} \leftarrow \mathcal{R}_{D_\theta}^{(i)}(\mathbf{x}^{(i)}, t_{i:i+1})$, with

$$\mathcal{R}_{D_\theta}^{(i)}(\mathbf{x}^{(i)}, t_{i:i+1}) := \hat{\mathbf{x}}^{(i)} + \frac{h}{2t_{i+1}} \left[\hat{\mathbf{x}}^{(i)} + (h + t_{i+1})d_i - \underbrace{D_\theta(\hat{\mathbf{x}}^{(i)} + hd_i, t_{i+1})}_{\text{Denoiser after Euler step}} \right] \quad (3)$$

Where $d_i := f(\hat{\mathbf{x}}^{(i)}, t_i(1 + \gamma))$ is as defined in line 1 of Algorithm 1 and γ is a hyperparameter controlling the amount of additional injected noise whose scale is determined by the S_{noise} hyperparameter. And $\hat{\mathbf{x}}^{(i)}$ is the current image with the added noise. Formally, we would like to claim that the distribution of the output $\mathbf{x}^{(N)}$ satisfies CoM, and we visualize the evolution of the norms of these quantities through the sampling process in Figure 4 to further illuminate our argument about the 1-Lipschitzness of the generative process.

3.3 Classification and Gaussian Universality

We cover Gaussian universality in the context of linear multiclass classification following the framework described in Ghane et al. [2024] and extend it to an arbitrary number of classes. As we will see, results of Ghane et al. [2024] and other known Gaussian universality results operate in an idealized setting that does not appear to be applicable to the covariance matrices estimated from the diffusion-generated images (Figure 6). Nevertheless, we observe empirically that universality holds in the latter setting as well, hence raising a challenge of relaxing the assumptions of the existing universality results to make them more practical. We outline the corresponding notation and challenge below.

- Consider data $\mathbf{x} \in \mathbb{R}^d$ being generated according to a mixture distribution with k classes $\mathbb{P} = \sum_{i=1}^k \theta_i \mathbb{P}_i$ for $0 \leq \theta_i \leq 1$ and $\sum_{i=1}^k \theta_i = 1$. For a sample \mathbf{x} from \mathbb{P}_i , i.e the i 'th class, we assign a label $\mathbf{y} \in \mathbb{R}^k$, to be $\mathbf{y} := \mathbf{e}_i$ (one-hot encoding). We consider a linear classifier $\mathbf{W} \in \mathbb{R}^{d \times k}$ with columns \mathbf{w}_ℓ for $\ell \in [k]$, where for a given datapoint \mathbf{x} , we classify \mathbf{x} based on

$$\arg \max_{\ell \in [k]} \mathbf{w}_\ell^T \mathbf{x}$$

The generalization error of a classifier \mathbf{W} on this task is defined as follows:

$$\sum_{i=1}^k \theta_i \mathbb{P} \left(i \neq \arg \max_{\ell \in [k]} \mathbf{w}_\ell^T \mathbf{x} \mid \mathbf{x} \sim \mathbb{P}_i \right)$$

- Given a training dataset $\{\mathbf{x}_i, \mathbf{y}_i\}_{i=1}^n$ with n samples, where each class has $n_i \approx \theta_i n$ samples, we construct the data matrix $\mathbf{X} \in \mathbb{R}^{n \times d}$ and the label matrix $\mathbf{Y} \in \mathbb{R}^{n \times k}$

$$\mathbf{X} = \begin{pmatrix} \mathbf{x}_1^T \\ \mathbf{x}_2^T \\ \vdots \\ \mathbf{x}_n^T \end{pmatrix}, \quad \mathbf{Y} = \begin{pmatrix} \mathbf{y}_1^T \\ \mathbf{y}_2^T \\ \vdots \\ \mathbf{y}_n^T \end{pmatrix}$$

Without loss of generality, we can rearrange the rows of \mathbf{X} to group samples from the same class together.

We also consider a Gaussian matrix $\mathbf{G} \in \mathbb{R}^{n \times d}$ whose rows have the same mean and covariances of the corresponding rows in \mathbf{X} . We sometimes refer to this statement as \mathbf{G} matching \mathbf{X} . In

other words, \mathbf{G} is a matrix of data sampled from the Gaussian mixture model (GMM) defined via $\sum_{i=1}^k \theta_i \mathcal{N}(\boldsymbol{\mu}_i, \boldsymbol{\Sigma}_i)$ where $\boldsymbol{\mu}_i = \mathbb{E}_{\mathbb{P}_i} \mathbf{x}$ and $\boldsymbol{\Sigma}_i = \mathbb{E}_{\mathbb{P}_i} \mathbf{x} \mathbf{x}^T - \boldsymbol{\mu}_i \boldsymbol{\mu}_i^T$ for \mathbf{x} belonging to class i . To train for \mathbf{W} , we minimize $\|\mathbf{Y} - \mathbf{X}\mathbf{W}\|_F^2$ by running SGD with a constant stepsize. By the implicit bias property of SGD Gunasekar et al. [2018], Azizan and Hassibi [2018] for linear models, we observe that the iterations of SGD initialized from some \mathbf{W}_0 converge to the optimal solution of the following optimization problem

$$\min_{\mathbf{W} \in \mathbb{R}^{d \times k}} \|\mathbf{W} - \mathbf{W}_0\|_F^2 \quad (4)$$

$$s.t. \quad \mathbf{X}\mathbf{W} = \mathbf{Y} \quad (5)$$

Then it is known Ghane et al. [2024] that under the list of technical Assumptions 1 listed below the \mathbf{W} obtained through running SGD on the data matrix \mathbf{X} has asymptotically the same performance (generalization error) as a $\tilde{\mathbf{W}}$ obtained through running SGD on the corresponding Gaussian matrix \mathbf{G} , that is $\tilde{\mathbf{W}}$ solving the following optimization problem:

$$\min_{\tilde{\mathbf{W}} \in \mathbb{R}^{d \times k}} \|\tilde{\mathbf{W}} - \mathbf{W}_0\|_F^2$$

$$s.t. \quad \mathbf{G}\tilde{\mathbf{W}} = \mathbf{Y}$$

In other words,

Theorem 1. *The following holds asymptotically under Assumptions 1 :*

$$\left| \sum_{i=1}^k \theta_i \mathbb{P} \left(i \neq \arg \max_{\ell \in [k]} \mathbf{W}_\ell^T \mathbf{x} \mid \mathbf{x} \sim \mathbb{P}_i \right) - \sum_{i=1}^k \theta_i \mathbb{P} \left(i \neq \arg \max_{\ell \in [k]} \tilde{\mathbf{W}}_\ell^T \mathbf{g} \mid \mathbf{g} \sim \mathcal{N}(\boldsymbol{\mu}_i, \boldsymbol{\Sigma}_i) \right) \right| \rightarrow 0$$

The required assumptions are as follows:

Assumptions 1. *Let \mathbf{x} be any row of \mathbf{X} and $\boldsymbol{\mu}$ be its mean. Then:*

- $\|\boldsymbol{\mu}\|_2 = O(1)$
- For any deterministic vector $\mathbf{v} \in \mathbb{R}^d$, and $q \in \mathbb{N}$, $q \leq 6$, there exists a constant $K > 0$ such that $\mathbb{E}_{\mathbf{x}} |(\mathbf{x} - \boldsymbol{\mu})^T \mathbf{v}|^q \leq K \frac{\|\mathbf{v}\|_2^q}{d^{q/2}}$
- For any deterministic matrix $\mathbf{C} \in \mathbb{R}^{d \times d}$ of bounded operator norm we have $\text{Var}(\mathbf{x}^T \mathbf{C} \mathbf{x}) \rightarrow 0$ as $d \rightarrow \infty$
- $s_{\min}(\mathbf{X}\mathbf{X}^T) = \Omega(1)$ with high probability where $s_{\min}(\cdot)$ is the smallest singular value.

3.4 Limitations of current universality results

Assumptions 1 hold, for example, for any sub-Gaussian \mathbf{x} with mean and covariance satisfying $\|\boldsymbol{\mu}\| = O(1)$ and $\frac{c\mathbf{I}_d}{d} \leq \boldsymbol{\Sigma}^{\frac{1}{2}} \leq \frac{C\mathbf{I}_d}{d}$ (see Remark 5 in Ghane et al. [2024] for details). However, assuming that $\frac{c\mathbf{I}_d}{d} \leq \boldsymbol{\Sigma}^{\frac{1}{2}} \leq \frac{C\mathbf{I}_d}{d}$ is crucial here, as otherwise one can take a Gaussian \mathbf{x} with $\boldsymbol{\Sigma} = \text{diag}(1, \frac{1}{4}, \dots, \frac{1}{d^2})$ and $\boldsymbol{\mu} = 0$ and notice that $\text{Var}(\|\mathbf{x}\|^2) = \text{Tr}(\boldsymbol{\Sigma}^2) - \text{Tr}(\boldsymbol{\Sigma})^2$ converges to a strictly positive number, violating the third part of Assumptions 1 for $\mathbf{C} = \mathbf{I}_d$, while \mathbf{x} is normalized correctly in the sense that $\mathbb{E}_{\mathbf{x}} \|\mathbf{x}\|^2 = \text{Tr}(\boldsymbol{\Sigma}) = O(1)$.

Unfortunately, as can be seen in Figure 6, the spectra of diffusion-generated images look qualitatively similar to the "power law" $\boldsymbol{\Sigma} = \text{diag}(1, \frac{1}{4}, \dots, \frac{1}{d^2})$, meaning that Theorem 1 does not apply in

this setting. Moreover, to the best of the authors’ knowledge, such covariance matrices break the assumptions commonly made in papers focusing on universality for *regression*, which is usually simpler to study. For example, Montanari and Saeed [2022] also have to assume $\frac{C\mathbf{I}_d}{d} \leq \Sigma^{\frac{1}{2}} \leq \frac{C\mathbf{I}_d}{d}$ to get concrete results for over-parametrized regression (cf. Theorem 5 in Montanari and Saeed [2022]). Despite this, as can be seen in the next section, the universality of the classification error does not break thus posing an interesting challenge of relaxing Assumptions 1 in Theorem 1.

While the theoretical result from Ghane et al. [2024] applied to the objectives of form (4), in practice one usually adds a softmax function $S(\mathbf{z}_1, \dots, \mathbf{z}_k) = (\dots, \frac{e^{\mathbf{z}_i}}{\sum e^{\mathbf{z}_i}}, \dots)$

$$\begin{aligned} \min_{\mathbf{W} \in \mathbb{R}^{d \times k}} \quad & \|\mathbf{W} - \mathbf{W}_0\|_F^2 \\ \text{s.t.} \quad & S(\mathbf{X}\mathbf{W}) \approx \mathbf{Y} \end{aligned} \tag{6}$$

Here, the approximate equality comes from the fact that the coordinates of the range of the softmax cannot turn exactly into zeros but will be very close to it on the training data if one fits the objective (6). Since this objective is of much greater practical interest than (4) and has better convergence properties, we add softmax into the objective for numerical validation of universality in the next section. Note that, from theoretical standpoint, it raises the question of incorporating softmax into the framework of Theorem 1.

3.5 Main Results

To explain why diffusion models do not perform well at generating heavy-tailed data, we prove the following result:

Theorem 2. *Assume that the denoiser $D_\theta(\mathbf{x}^{(i)}, t_{i:i+1})$ is trained in such a way that $\|\mathcal{R}_{D_\theta}^{(i)}(\mathbf{x}^{(i)}, t_{i:i+1})\| \leq \|\mathbf{x}^{(i)}\|$ under the notation from (2) holds for every sampling step with high probability w.r.t the randomness in ϵ_i . Then the resulting output $\mathbf{x}^{(N)}$ satisfies the CoM property from Definition 1 for $C = 2$ and $\sigma = t_0$, where $\mathbf{x}^{(0)} \sim \mathcal{N}(0, t_0^2 \mathbf{I}_d)$.*

The assumption $\|\mathcal{R}_{D_\theta}^{(i)}(\mathbf{x}, t_{i:i+1})\| \leq \|\mathbf{x}\|$ might come out as very specific. In addition, it was not clear to us how to analytically verify that it is true. Nevertheless, we justify it by the following empirical observation. Understanding mathematically why Empirical Observation 1 holds thus poses an interesting challenge as well.

Empirical Observation 1. *Each sampling step $\mathbf{x}^{(i+1)} = \mathcal{R}_{D_\theta}^{(i)}(\mathbf{x}^{(i)}, t_{i:i+1})$ of the Algorithm 1 decreases norms, i.e. $\|\mathbf{x}^{(i)}\| \leq \|\mathbf{x}^{(i-1)}\|$ is satisfied throughout the reverse process. The results of the corresponding experiments can be found in Figure 4.*

As explained in Subsection 3.3, CoM property is insufficient for concluding universality from any of the known universality theorems unless the upper bound from the right hand side of Definition 1 goes to 0. Nevertheless, our experiments suggest that universality holds for diffusion-generated images despite this technicality. As such, we would like to report it as an empirical observation and present the question of extending Theorem 1 to capture more complicated covariance matrices Σ such as the power law as an open question for future theory works.

Empirical Observation 2. *The distributions of images generated via EDM diffusion models satisfy Gaussian Universality of the test error in the sense of the conclusion of Theorem 1 for weights trained via minimizing $\|\mathbf{Y} - S(\mathbf{X}\mathbf{W})\|_2^2$ using SGD. The experiments are presented in Figure 5 preceded by the description of the setup.*

4 Experiments

We conduct a series of experiments ¹ where we train linear classifiers on diffusion-generated images and on samples from a Gaussian Mixture Model (GMM) with matching mean and covariance. We also empirically investigate the concentration of these images. Throughout all of our experiments, we utilize the trained conditional diffusion model checkpoint from EDM Karras et al. [2022], which uses the ADM architecture Dhariwal and Nichol [2021] and was trained on Imagenet64 (Imagenet-1k downsampled to 64x64 pixels). Moreover, we sample according to the EDM stochastic sampler outlined in 1, using the recommended settings.

We take a 20 class subset of the 1000 Imagenet classes and sample 10240 images from the diffusion model. Our data is of dimension $12288 = (3 \text{ RGB channels} \times 64 \text{ pixels} \times 64 \text{ pixels})$. We then fit a GMM with all these samples to create the corresponding Gaussian data. Specifically, these classes are: Baseball, Cauliflower, Church, Coral Reef, English Springer, French Horn, Garbage Truck, Goldfinch, Kimono, Mountain Bike, Patas Monkey, Pizza, Planetarium, Polaroid, Racer, Salamandra, Tabby, Tench, Trimaran, Volcano. Figure 2 presents samples from our dataset.

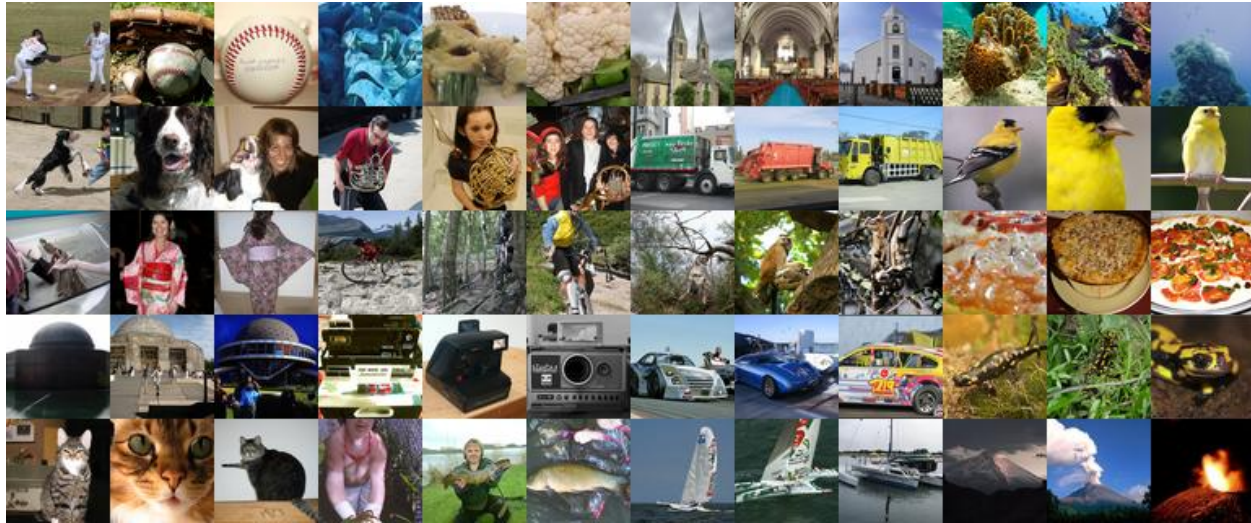


Figure 2: Samples from conditional diffusion model with ADM architecture Dhariwal and Nichol [2021] using the checkpoint and sampler settings from Karras et al. [2022], trained on Imagenet64.

We empirically investigate the concentration of norms throughout the sampling process. Following the recommendations of Karras et al. [2022], the diffusion sampling process of $N = 256$ steps, with $\sigma(t) = t$, begins with isotropic Gaussian noise with scale $t_{max} := t_0 = 80$. The noise schedule is constructed as $t_{i < N} = \left(t_{max}^{\frac{1}{\rho}} + \frac{i}{N-1} \left(t_{min}^{\frac{1}{\rho}} - t_{max}^{\frac{1}{\rho}} \right) \right)^{\rho}$ with $t_{min} := t_{N-1} = 0.002$ and final noise scale $t_N = 0$. Here, $\rho = 7$ is a hyperparameter observed to improve image quality.

¹We release all of our code for these experiments at <https://github.com/abao1999/diffusion-gmm>.

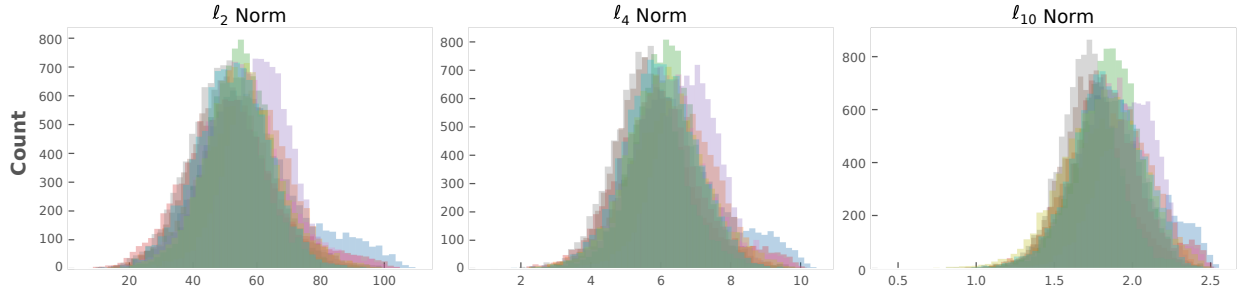


Figure 3: The distribution of the ℓ_2 , ℓ_4 and ℓ_{10} norms of diffusion-generated images for 10 classes of Imagenet64 included in our experiments, computed over 10240 samples per class.

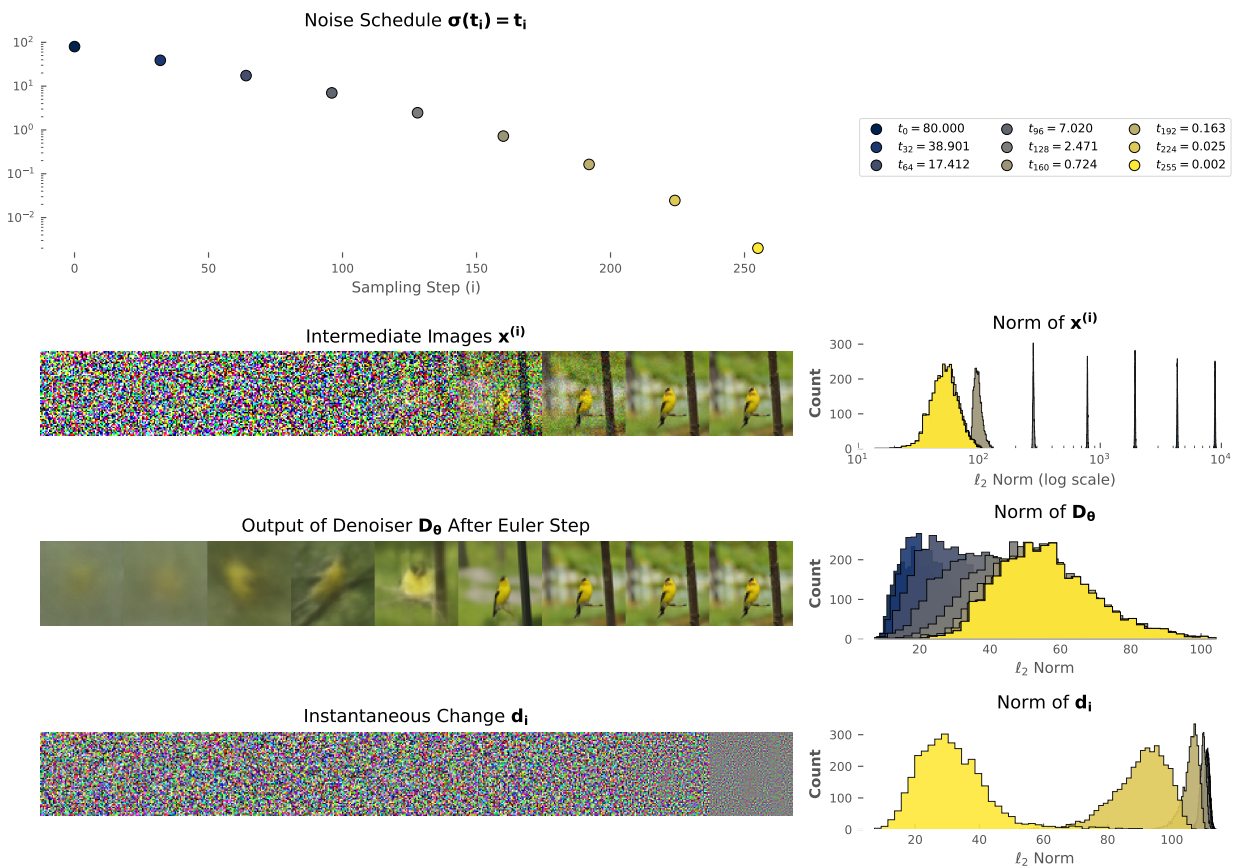


Figure 4: The evolution of the ℓ_2 norms through the stochastic sampling process 1. The noise schedule and sampler settings are as prescribed in Karras et al. [2022].

See Figure 9 in the Appendix section E for further discussion on the sampling process.

4.1 Linear Classifier Experiments

We train linear classifiers on our dataset of diffusion-generated images and on the corresponding Gaussian data sampled from a GMM fitted on 10240 diffusion-generated images per class. Following the setting of subsection 3.3, we use SGD as our optimizer and mean squared error (MSE) as our loss criterion. For multi-class classification, we use a softmax activation on the logits and compute the MSE loss against the one-hot-encoded class labels. For binary classification, we compute the MSE loss on the logit after sigmoid activation. This regression on predicted class probabilities is done in practice when working with soft (noisy) labels or in the context of knowledge distillation.

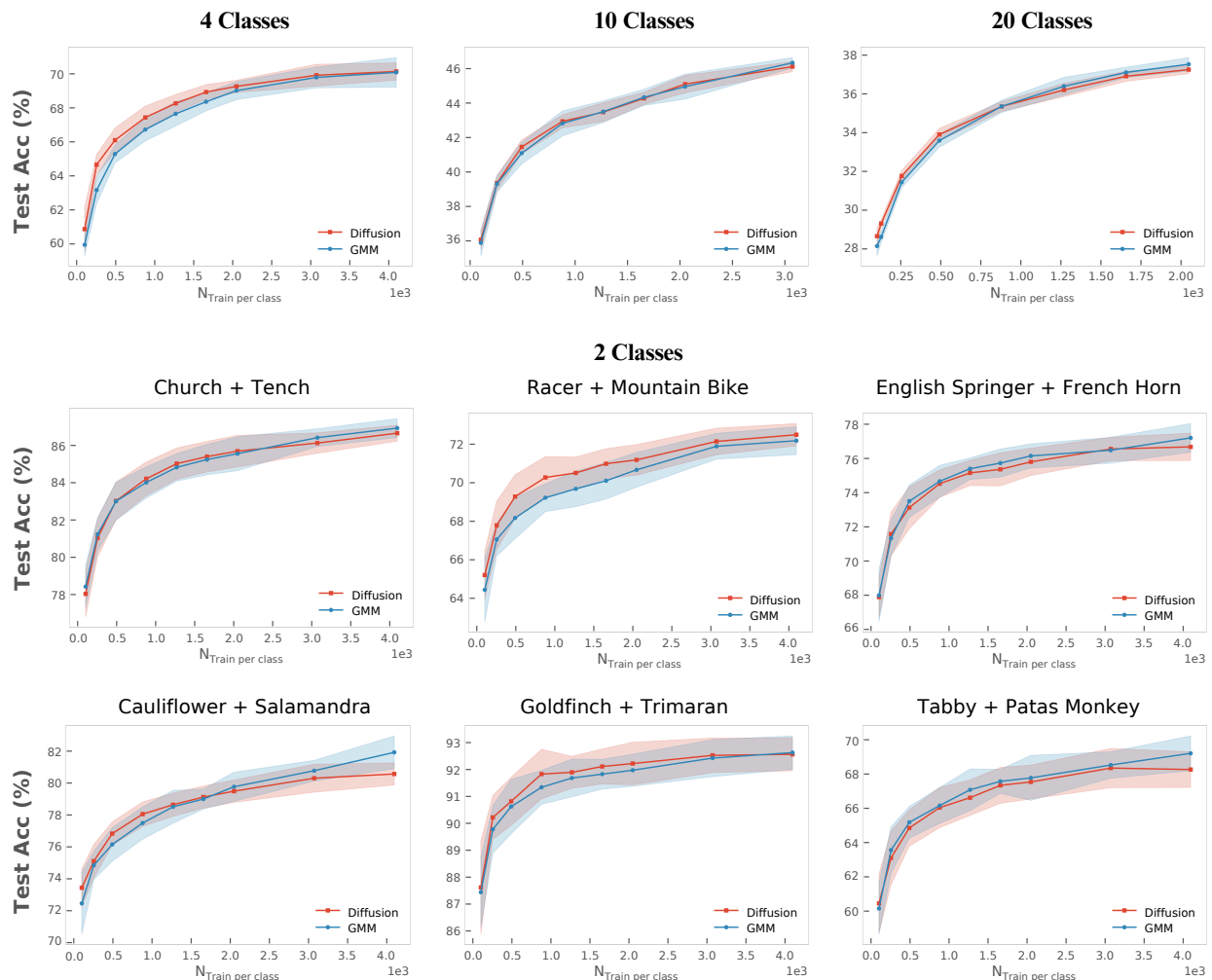


Figure 5: Linear classifier accuracies for diffusion-generated images (Red) and GMM samples (Blue). **Top Row:** Accuracies for 4, 10, and 20 class subsets of Baseball, Cauliflower, Church, Coral Reef, English Springer, French Horn, Garbage Truck, Goldfinch, Kimono, Mountain Bike, Patas Monkey, Pizza, Planetarium, Polaroid, Racer, Salamandra, Tabby, Tench, Trimaran, Volcano. **Middle/Bottom Rows:** Binary classification accuracies for pairs of classes.

We compare the accuracies achieved by linear classification on the diffusion-generated images versus

the GMM samples, when varying the size of the training set between 128 and 4096 samples per class. Figure 5 presents the results of 10-20 independent runs per training data split, with a different random seed for each run. Thus, for each run, a unique pseudorandom generator state determines weight initialization in addition to the sampling and minibatch shuffling of $N_{\text{train per class}} \in [128, 4096]$ samples from our dataset of 10240 samples per class for diffusion-generated images and GMM samples. Likewise, we fix the size of our held-out test set to $N_{\text{test per class}} = 1024$, randomly sampled according to each run’s unique random state from a separate subset of our dataset to ensure no overlap with the training set.

To robustly achieve the best possible linear classification performance, we perform an extensive sweep² over a range of learning rates between $[1e - 4, 0.1]$ and learning rate schedulers, while ensuring convergence with respect to the test loss, and no overfitting on the training set. For practical reasons, we use a Cosine Annealing learning rate schedule to speed up convergence, which we find achieves the best performance. The main conclusion from our linear classifier experiments, as summarized in Figure 5, is that the accuracies match for linear classifiers trained on diffusion-generated images and the corresponding Gaussian data, for a range of training set sizes and class subsets. At large values of $N_{\text{train per class}}$ we begin to see a divergence in the accuracies, which we attribute to the estimation gap from computing the mean and covariance from a finite number of samples for the Gaussian data. The choice of MSE loss on one-hot-encoded labels may seem unconventional for a classification task but is done to match the setting of 3.3. In Appendix Section A we re-run these experiments with the more conventional Cross Entropy loss and also observe a match in accuracies.

5 Conclusion

In this work, we focus on characterizing the mathematical properties of images generated by diffusion models by examining the generalization error of the classification tasks. We are motivated by the fact that characterizing the generalization error and performance of neural networks precisely remains one of most challenging problems in modern machine learning. In fact, most theoretical works have focused on analyzing models under specific assumptions about data distribution, such as isotropic Gaussianity even though real-world datasets are almost never Gaussian. As such, we choose to study theoretical properties of the diffusion-generated distributions instead as an approximation to real-world distributions more amenable to analyses. Future directions include extending the universality results to accommodate for more general covariance matrices, incorporating training with softmax into the universality framework and providing a rigorous proof of the contractivity of the sampling process.

²We make our classifier sweeps publicly available at <https://wandb.ai/abao/diffusion-gmm>

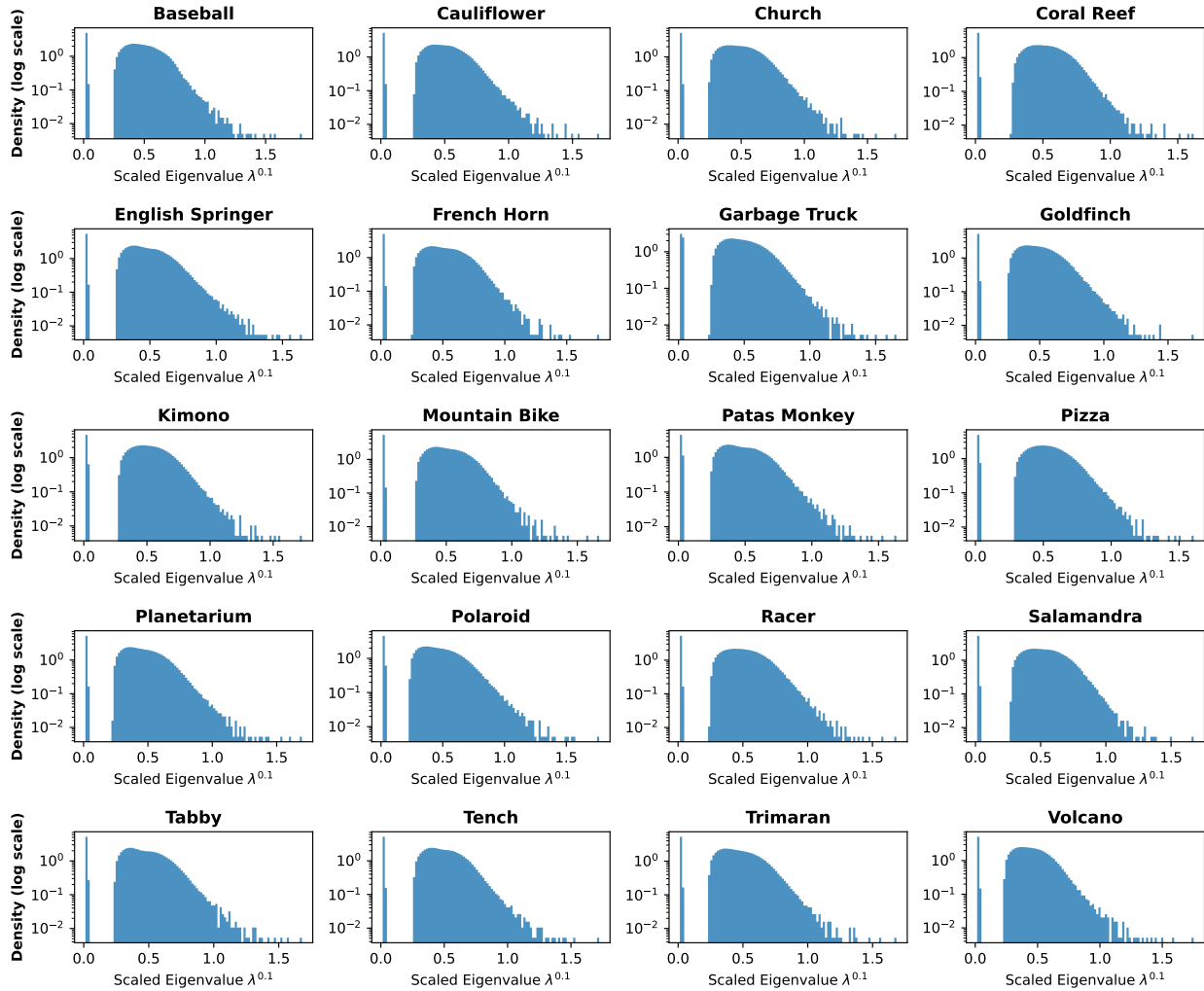


Figure 6: Spectra of the covariance matrices computed from 10240 diffusion-generated images for each of the 20 classes of *Imagenet64* considered in our experiments. Note that for sake of clearer presentation, we have scaled the eigenvalues by an exponent 0.1.

References

- J. Austin, D. D. Johnson, J. Ho, D. Tarlow, and R. Van Den Berg. Structured denoising diffusion models in discrete state-spaces. *Advances in Neural Information Processing Systems*, 34:17981–17993, 2021.
- N. Azizan and B. Hassibi. Stochastic gradient/mirror descent: Minimax optimality and implicit regularization. *arXiv preprint arXiv:1806.00952*, 2018.
- S. G. Bobkov. On concentration of distributions of random weighted sums. *Annals of probability*, pages 195–215, 2003.
- B. Bordelon, A. Canatar, and C. Pehlevan. Spectrum dependent learning curves in kernel regression and wide neural networks. In *International Conference on Machine Learning*, pages 1024–1034. PMLR, 2020.
- S. Chen, S. Chewi, J. Li, Y. Li, A. Salim, and A. R. Zhang. Sampling is as easy as learning the score: theory for diffusion models with minimal data assumptions. *arXiv preprint arXiv:2209.11215*, 2022.
- F.-A. Croitoru, V. Hondru, R. T. Ionescu, and M. Shah. Diffusion models in vision: A survey. *IEEE Transactions on Pattern Analysis and Machine Intelligence*, 45(9):10850–10869, 2023.
- Y. Dandi, L. Stephan, F. Krzakala, B. Loureiro, and L. Zdeborová. Universality laws for gaussian mixtures in generalized linear models. *Advances in Neural Information Processing Systems*, 36, 2024.
- P. Dhariwal and A. Nichol. Diffusion models beat gans on image synthesis. *Advances in neural information processing systems*, 34:8780–8794, 2021.
- D. C. Dowell, C. R. Alexander, E. P. James, S. S. Weygandt, S. G. Benjamin, G. S. Manikin, B. T. Blake, J. M. Brown, J. B. Olson, M. Hu, et al. The high-resolution rapid refresh (hrrr): An hourly updating convection-allowing forecast model. part i: Motivation and system description. *Weather and Forecasting*, 37(8):1371–1395, 2022.
- F. Gerace, F. Krzakala, B. Loureiro, L. Stephan, and L. Zdeborová. Gaussian universality of perceptrons with random labels. *Physical Review E*, 109(3):034305, 2024.
- R. Ghane, D. Akhtiamov, and B. Hassibi. Universality in transfer learning for linear models. *arXiv preprint arXiv:2410.02164*, 2024.
- M. Goldblum, A. Anandkumar, R. Baraniuk, T. Goldstein, K. Cho, Z. C. Lipton, M. Mitchell, P. Nakkiran, M. Welling, and A. G. Wilson. Perspectives on the state and future of deep learning—2023. *arXiv preprint arXiv:2312.09323*, 2023.
- S. Gunasekar, J. Lee, D. Soudry, and N. Srebro. Characterizing implicit bias in terms of optimization geometry. In *International Conference on Machine Learning*, pages 1832–1841. PMLR, 2018.
- J. Ho, A. Jain, and P. Abbeel. Denoising diffusion probabilistic models. In H. Larochelle, M. Ranzato, R. Hadsell, M. Balcan, and H. Lin, editors, *Advances in Neural Information Processing Systems*, volume 33, pages 6840–6851. Curran Associates, Inc., 2020. URL <https://proceedings.neurips.cc/paper/2020/file/4c5bcfec8584af0d967f1ab10179ca4b-Paper.pdf>.

- A. Jacot, B. Simsek, F. Spadaro, C. Hongler, and F. Gabriel. Kernel alignment risk estimator: Risk prediction from training data. *Advances in neural information processing systems*, 33:15568–15578, 2020.
- T. Karras, M. Aittala, T. Aila, and S. Laine. Elucidating the design space of diffusion-based generative models. *Advances in neural information processing systems*, 35:26565–26577, 2022.
- H. Kim, G. Papamakarios, and A. Mnih. The lipschitz constant of self-attention. In *International Conference on Machine Learning*, pages 5562–5571. PMLR, 2021.
- D. Kingma, T. Salimans, B. Poole, and J. Ho. Variational diffusion models. *Advances in neural information processing systems*, 34:21696–21707, 2021.
- Z. Kong, W. Ping, J. Huang, K. Zhao, and B. Catanzaro. Diffwave: A versatile diffusion model for audio synthesis. *arXiv preprint arXiv:2009.09761*, 2020.
- M. Ledoux. Concentration of measure and logarithmic sobolev inequalities. In *Seminaire de probabilites XXXIII*, pages 120–216. Springer, 2006.
- G. Li, Y. Wei, Y. Chi, and Y. Chen. A sharp convergence theory for the probability flow odes of diffusion models. *arXiv preprint arXiv:2408.02320*, 2024a.
- X. Li, Y. Dai, and Q. Qu. Understanding generalizability of diffusion models requires rethinking the hidden gaussian structure. In *The Thirty-eighth Annual Conference on Neural Information Processing Systems*, 2024b. URL <https://openreview.net/forum?id=Sk2duBGvrK>.
- B. Loureiro, C. Gerbelot, H. Cui, S. Goldt, F. Krzakala, M. Mezard, and L. Zdeborová. Learning curves of generic features maps for realistic datasets with a teacher-student model. *Advances in Neural Information Processing Systems*, 34:18137–18151, 2021a.
- B. Loureiro, G. Sicuro, C. Gerbelot, A. Pacco, F. Krzakala, and L. Zdeborová. Learning gaussian mixtures with generalized linear models: Precise asymptotics in high-dimensions. *Advances in Neural Information Processing Systems*, 34:10144–10157, 2021b.
- A. Montanari and B. N. Saeed. Universality of empirical risk minimization. In *Conference on Learning Theory*, pages 4310–4312. PMLR, 2022.
- A. Mousavi-Hosseini, T. K. Farghly, Y. He, K. Balasubramanian, and M. A. Erdogdu. Towards a complete analysis of langevin monte carlo: Beyond poincaré inequality. In *The Thirty Sixth Annual Conference on Learning Theory*, pages 1–35. PMLR, 2023.
- P. Nakkiran. *Towards an empirical theory of deep learning*. PhD thesis, Harvard University, 2021.
- K. Pandey, J. Pathak, Y. Xu, S. Mandt, M. Pritchard, A. Vahdat, and M. Mardani. Heavy-tailed diffusion models. *arXiv preprint arXiv:2410.14171*, 2024.
- L. Pesce, F. Krzakala, B. Loureiro, and L. Stephan. Are gaussian data all you need? the extents and limits of universality in high-dimensional generalized linear estimation. In *International Conference on Machine Learning*, pages 27680–27708. PMLR, 2023.
- M. Refinetti, A. Ingrosso, and S. Goldt. Neural networks trained with sgd learn distributions of increasing complexity. In *International Conference on Machine Learning*, pages 28843–28863. PMLR, 2023.

- R. Rombach, A. Blattmann, D. Lorenz, P. Esser, and B. Ommer. High-resolution image synthesis with latent diffusion models. In *Proceedings of the IEEE/CVF conference on computer vision and pattern recognition*, pages 10684–10695, 2022.
- M. Rudelson and R. Vershynin. Hanson-wright inequality and sub-gaussian concentration. 2013.
- M. E. A. Seddik, C. Louart, M. Tamaazousti, and R. Couillet. Random matrix theory proves that deep learning representations of gan-data behave as gaussian mixtures. In *Proceedings of the 37th International Conference on Machine Learning, ICML'20*. JMLR.org, 2020.
- J. Sohl-Dickstein, E. Weiss, N. Maheswaranathan, and S. Ganguli. Deep unsupervised learning using nonequilibrium thermodynamics. In F. Bach and D. Blei, editors, *Proceedings of the 32nd International Conference on Machine Learning*, volume 37 of *Proceedings of Machine Learning Research*, pages 2256–2265, Lille, France, 07–09 Jul 2015. PMLR.
- J. Song, C. Meng, and S. Ermon. Denoising diffusion implicit models. *arXiv preprint arXiv:2010.02502*, 2020.
- Y. Song and S. Ermon. Generative modeling by estimating gradients of the data distribution. *Advances in neural information processing systems*, 32, 2019.
- Y. Song, J. Sohl-Dickstein, D. P. Kingma, A. Kumar, S. Ermon, and B. Poole. Score-based generative modeling through stochastic differential equations. In *International Conference on Learning Representations*, 2021. URL <https://openreview.net/forum?id=PxtTIG12RRHS>.
- C. Thrampoulidis, S. Oymak, and M. Soltanolkotabi. Theoretical insights into multiclass classification: A high-dimensional asymptotic view. *Advances in Neural Information Processing Systems*, 33:8907–8920, 2020.
- R. Vershynin. *High-dimensional probability: An introduction with applications in data science*, volume 47. Cambridge university press, 2018.
- L. Yang, Z. Zhang, Y. Song, S. Hong, R. Xu, Y. Zhao, W. Zhang, B. Cui, and M.-H. Yang. Diffusion models: A comprehensive survey of methods and applications. *ACM Computing Surveys*, 56(4): 1–39, 2023.

A Classifier Experiments with Cross Entropy Loss

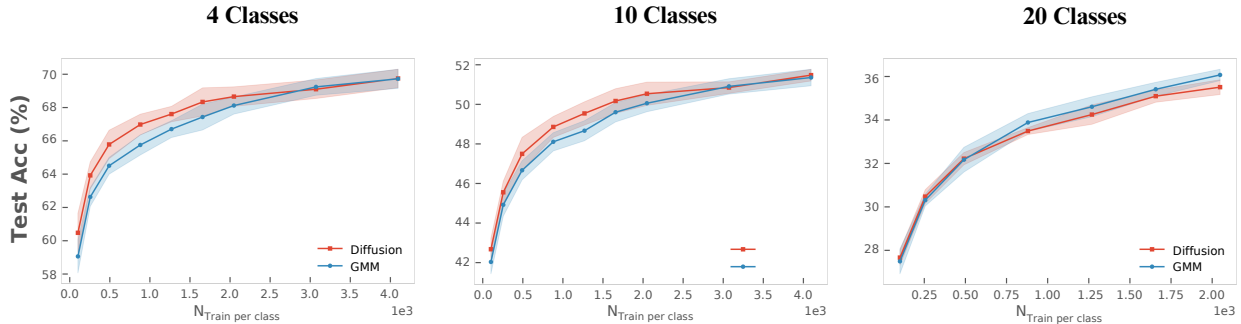


Figure 7: Accuracies for linear classifier trained with Cross Entropy Loss, for diffusion-generated images (Red) and GMM samples (Blue). We consider 4, 10, and 20 class subsets of Baseball, Cauliflower, Church, Coral Reef, English Springer, French Horn, Garbage Truck, Goldfinch, Kimono, Mountain Bike, Patas Monkey, Pizza, Planetarium, Polaroid, Racer, Salamandra, Tabby, Tench, Trimaran, Volcano

When training linear classifiers with the more conventional choice of Cross Entropy Loss, we also observe a match in the accuracies between classifiers trained on diffusion-generated images and on the corresponding Gaussian data. We did not perform as extensive a sweep for this setting, and expect the match to improve upon doing so.

B Proof of Theorem 2

We rely on the following proposition, claiming that the image of an exponentially concentrated distribution under a Lipschitz transformation remains exponentially concentrated, albeit with different constants. It follows trivially from the definition of concentration but is nonetheless crucial for our purposes:

Proposition 2. *Let \mathbf{x} satisfy Definition 1 with constants C, σ and assume that $\mathcal{G} : \mathbb{R}^d \rightarrow \mathbb{R}^D$ is L -Lipschitz. Then $\mathcal{G}(\mathbf{x})$ satisfies CoM from Definition 1 as well with constants $C, L\sigma$.*

Now, recall that the images are generated step by step according to:

$$\mathbf{x}_0 \approx \mathbf{x}^{(N)} = \mathcal{R}_{D_\theta}^{(N-1)}(\mathcal{R}_{D_\theta}^{(N-2)}(\dots \mathcal{R}_{D_\theta}^{(0)}(\mathbf{x}^{(0)}, t_{0:1}) \dots), t_{N-2:N-1}), t_{N-1:N}) \quad (7)$$

We will prove that each \mathbf{x}_i satisfies the CoM of measure property by induction by $i = 0, \dots, N$:

- Basis $i = 0$ follows from Proposition 1
- Step $i \rightarrow i + 1$ would follow by applying Proposition 2 with $L = 1$ to $\mathbf{x}^{(i+1)} = \mathcal{R}_{D_\theta}^{(i)}(\mathbf{x}^{(i)}, t_{i:i+1})$ if we knew that $\mathcal{R}_{D_\theta}^{(i)}(\cdot, t_{i:i+1})$ is 1-Lipschitz. Since we already assume that $\mathcal{R}_{D_\theta}^{(i)}$ is norm-decreasing, it suffices to just prove that it is Lipschitz. The latter does not have to hold in general but in this case we make a specific assumption that $\mathcal{R}_{D_\theta}^{(i)}$ corresponds to a denoiser employing a UNET architecture. This is a neural network consisting of the following blocks:
 - *Fully-Connected Layers* with a Lipschitz activation function $\sigma = \text{SiLU}$ and a matrix of weights \mathbf{W} . These are Lipschitz functions with constant $\|\sigma\|_{\text{Lip}} \|\mathbf{W}\|_{\text{op}}$.

- *Convolutional Layers* with a filter \mathbf{W} . These are also Lipschitz functions with constant $\|\sigma\|_{Lip}\|\mathbf{W}\|_{op}$.
- *Self-Attention Layers* As shown in Kim et al. [2021], these are *not Lipschitz* over the entire domain. However, it can be seen from the same derivations that, if we restrict the domain to points from a distribution satisfying CoM, then it *is Lipschitz with high probability*. Thus, for our specific scenario, these are Lipschitz as well.
- *Max Pool, Average Pool, Group Normalization, Positional Embedding, Upsampling and Downsampling Layers*. All these layers are 1-Lipschitz.

We conclude that the mapping $\mathbf{x}^{(i)} \rightarrow \mathbf{x}^{(i+1)}$ is Lipschitz but, technically speaking, the constant is unbounded without the assumption that $\mathcal{R}_{D_\theta}^{(i)}$ does not increase norms. Moreover, since the sampling process involves N steps for a relatively big N , the Lipschitz constant of the mapping $\mathbf{x}_T \rightarrow \mathbf{x}_0$ might accumulate and explode unless the Lipschitz constant of each step is bounded by 1. While we could not prove directly that the latter is the case so far, we observed it to be the case in the simulations we have conducted (cf. Figure 4). As such, we decided to assume that the training is performed in such a manner that the sampling steps $\mathbf{x}^{(i)} \rightarrow \mathbf{x}^{(i+1)}$ are all 1-Lipschitz mappings for the scope of the present work. In addition, we can prove that the same conclusion holds if we only assume that each \mathcal{R}_i is norm-decreasing for large enough $t > K$ for a constant K . This follows automatically from the following result, that we could not find in the literature:

Theorem 3. *If $(x, y) \sim \Pi$ where Π is a joint distribution with marginals, $\pi_{1\#}\Pi = p_1$ and $\pi_{2\#}\Pi = p_2$ and p_1 and p_2 are two distributions satisfying CoM, then (x, y) also satisfies CoM.*

Proof. The proof technique is adopted from Ledoux [2006]. We also extend that result to accommodate for arbitrary coupling on (x, y) . For every L -Lipschitz function $f : \mathbb{R}^d \times \mathbb{R}^d \rightarrow \mathbb{R}$, we have from triangle inequality

$$\mathbb{P}(|f(x, y) - \mathbb{E}_\Pi f(x, y)| > 2t) \leq \mathbb{P}(|f(x, y) - \mathbb{E}_{p_1} f(x, y)| > t) + \mathbb{P}(|\mathbb{E}_{p_1} f(x, y) - \mathbb{E}_\Pi f(x, y)| > t) \quad (8)$$

For the first term in 8, we have that for the joint distribution Π

$$\begin{aligned} \mathbb{P}(|f(x, y) - \mathbb{E}_{p_1} f(x, y)| > t) &= \mathbb{E}_\Pi \mathbf{1}\{|f(x, y) - \mathbb{E}_{p_1} f(x, y)| > t\} = \mathbb{E}_{p_2} \mathbb{E}_{p_1|p_2} \mathbf{1}\{|f(x, y) - \mathbb{E}_{p_1} f(x, y)| > t\} \\ &= \mathbb{E}_{p_2} \mathbb{P}_{p_1|p_2}(|f(x, y) - \mathbb{E}_{p_1} f(x, y)| > t) \end{aligned}$$

Now we observe that for every y , $f(x, y)$ is also L -Lipschitz in x , thus by CoM

$$\mathbb{P}(|f(x, y) - \mathbb{E}_{p_1} f(x, y)| > t) = \mathbb{E}_{p_2} \mathbb{P}_{p_1|p_2}(|f(x, y) - \mathbb{E}_{p_1} f(x, y)| > t) \leq \mathbb{E}_{p_2} C e^{-\left(\frac{t}{L\sigma}\right)^2} = C e^{-\left(\frac{t}{L\sigma}\right)^2}$$

For the second term in 8, letting $g(y) := \mathbb{E}_{p_1} f(x, y)$, we observe that g is also Lipschitz, so by CoM for p_2 ,

$$\mathbb{P}(|\mathbb{E}_{p_1} f(x, y) - \mathbb{E}_\Pi f(x, y)| > t) \leq C e^{-\left(\frac{t}{L\sigma}\right)^2}$$

Summarizing, we obtain that:

$$\mathbb{P}(|f(x, y) - \mathbb{E}_\Pi f(x, y)| > 2t) \leq 2C e^{-\left(\frac{t}{L\sigma}\right)^2}$$

□

C Proof of Theorem 1

First note that we will utilize a multi-dimensional version of the CLT result of Bobkov [2003] (Corollary 2.5) which controls the following quantity for a matrix \mathbf{W} with "generic" column vectors:

$$\left| \mathbb{P}\left(i \neq \arg \max_{\ell \in [k]} \mathbf{W}_{\ell, \Phi_\lambda(\mathbf{X})}^T \mathbf{x} \mid \mathbf{x} \sim \mathbb{P}_i\right) - \mathbb{P}\left(i \neq \arg \max_{\ell \in [k]} \mathbf{W}_{\ell, \Phi_\lambda(\mathbf{X})}^T \mathbf{g} \mid \mathbf{x} \sim \mathbb{P}_i\right) \right|$$

This generalization follows by applying a union bound argument. For the main quantity of interest,

$$\left| \mathbb{P}\left(i \neq \arg \max_{\ell \in [k]} \mathbf{W}_{\ell, \Phi_\lambda(\mathbf{X})}^T \mathbf{x} \mid \mathbf{x} \sim \mathbb{P}_i\right) - \mathbb{P}\left(i \neq \arg \max_{\ell \in [k]} \mathbf{W}_{\ell, \Phi_\lambda(\mathbf{G})}^T \mathbf{g} \mid \mathbf{x} \sim \mathbb{P}_i\right) \right|$$

We would need to bound the following:

$$\left| \mathbb{P}\left(i \neq \arg \max_{\ell \in [k]} \mathbf{W}_{\ell, \Phi_\lambda(\mathbf{X})}^T \mathbf{g} \mid \mathbf{x} \sim \mathbb{P}_i\right) - \mathbb{P}\left(i \neq \arg \max_{\ell \in [k]} \mathbf{W}_{\ell, \Phi_\lambda(\mathbf{G})}^T \mathbf{g} \mid \mathbf{x} \sim \mathbb{P}_i\right) \right|$$

Which involves analyzing the covariance and the mean of $\mathbf{W}_{\ell, \Phi_\lambda(\mathbf{A})}^T \mathbf{g}$ for $\mathbf{A} = \mathbf{G}, \mathbf{X}$.

We know from Thrampoulidis et al. [2020] for the case of a GMM, (see Equation 2.7 in Thrampoulidis et al. [2020]) that the generalization error is characterized by the quantities $\boldsymbol{\mu}_\ell^T(\mathbf{w}_\ell - \mathbf{w}_{\ell'})$, and $\boldsymbol{\Sigma}_\ell^{1/2} \mathbf{S} \boldsymbol{\Sigma}_\ell^{1/2}$ where $(S_\ell)_{ij} := (\mathbf{w}_i - \mathbf{w}_j)^T (\mathbf{w}_i - \mathbf{w}_j)$ for $i, j \neq \ell$. Consider the following ridge regression objective:

$$\Phi_\lambda(\mathbf{A}) := \min_{\mathbf{W}} \frac{\lambda}{2} \|\mathbf{A}\mathbf{W} - \mathbf{Y}\|_F^2 + \|\mathbf{W}\|_F^2 = \sum_{\ell=1}^k \min_{\mathbf{w}_\ell} \frac{\lambda}{2} \|\mathbf{A}\mathbf{w}_\ell - \mathbf{y}_\ell\|_2^2 + \|\mathbf{w}_\ell\|_2^2$$

We denote the solution to the above optimization problem as $\mathbf{W}_{\Phi_\lambda(\mathbf{A})}$. Now in order to characterize $(S_\ell)_{ij}$, note that we need to understand the pairwise interaction of \mathbf{w}_i and \mathbf{w}_j and the decomposition provided cannot capture these quantities. To do this, we use the following identity:

$$\begin{aligned} & \min_{\mathbf{w}_i, \mathbf{w}_j} \frac{\lambda}{2} \|\mathbf{A}\mathbf{w}_i - \mathbf{y}_\ell\|_2^2 + \|\mathbf{w}_i\|_2^2 + \frac{\lambda}{2} \|\mathbf{A}\mathbf{w}_j - \mathbf{y}_\ell\|_2^2 + \|\mathbf{w}_j\|_2^2 \\ &= \min_{\mathbf{w}_i - \mathbf{w}_j, \mathbf{w}_i + \mathbf{w}_j} \frac{\lambda}{4} \|\mathbf{A}(\mathbf{w}_i + \mathbf{w}_j) - \mathbf{y}_\ell\|_2^2 + \|\mathbf{w}_i + \mathbf{w}_j\|_2^2 + \frac{\lambda}{4} \|\mathbf{A}(\mathbf{w}_i - \mathbf{w}_j) - \mathbf{y}_\ell\|_2^2 + \|\mathbf{w}_i - \mathbf{w}_j\|_2^2 \end{aligned}$$

And by studying the norms of $\boldsymbol{\Sigma}_\ell^{1/2}(\mathbf{w}_i \pm \mathbf{w}_j)$ we can understand $(S_\ell)_{ij}$. Note that in the argument above \mathbf{A} could be either \mathbf{X} and \mathbf{G} as a multi-dimensional CLT argument reduces the problem of universality of the test error on \mathbf{X} to \mathbf{G} and it only requires the first and second order statistics of \mathbf{X} . Note that by combining the results of Ghane et al. [2024] and the above identity, we observe that $|(S_\ell(\mathbf{X}))_{ij} - (S_\ell(\mathbf{G}))_{ij}| \xrightarrow{\mathbb{P}} 0$ for every λ . By a similar argument to Ghane et al. [2024], we observe that if $\Phi_\lambda(\mathbf{A}) \xrightarrow{\mathbb{P}} c_\lambda$ then $\sup_{\lambda>0} \Phi_\lambda(\mathbf{A}) \xrightarrow{\mathbb{P}} \sup_{\lambda>0} c_\lambda$. Combining this with a perturbation argument similar to Ghane et al. [2024] concludes the proof.

D Gram Spectrum

For each of the subsets of classes we considered for our multiclass linear classification experiments, we also investigated the spectrum of the gram matrix of the corresponding mixture distribution.

Using an equal number of samples per class, we construct a data matrix $X \in \mathbb{R}^{N \times D}$ where N is the total number of samples and $D = 12288$ is the dimensionality of each sample. Figure 8 presents the eigenvalue spectrum of the resulting Gram matrix $XX^T \in \mathbb{R}^{N \times N}$. As can be seen, we observe a very close match between the distributions of the eigenvalues of the Gram matrices for the diffusion-generated data and the corresponding GMM, but there is a slight mismatch for the smaller eigenvalues. We leave the question of finding out if there are any reasons for the latter mismatch apart from numerical inaccuracies for future work.

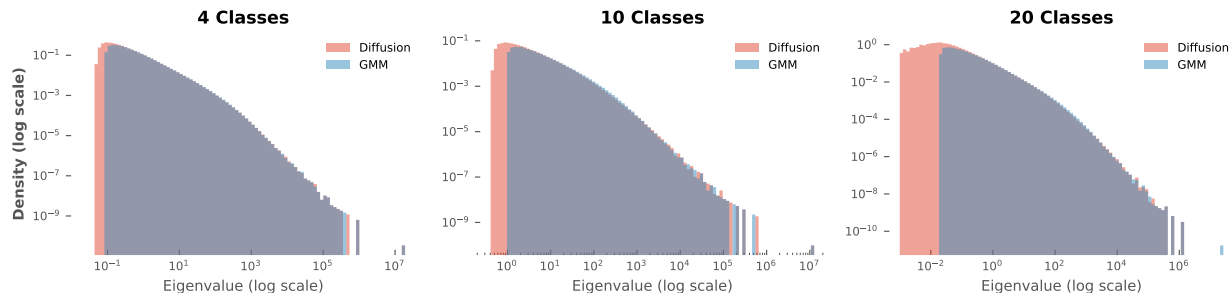


Figure 8: Spectra of Gram Matrices for balanced mixtures of samples from 4, 10, and 20 classes considered in the linear classification experiments. Computed for Diffusion (Red) and GMM (Blue). We use 2048 samples per class for 4 classes, and 512 samples per class for 10 and 20 classes.

E Sampling Process

In Figure 4, we plotted the evolution of the norms through the EDM sampling process. We now present further empirical evidence to show that the norms are decreasing with each sampling step.

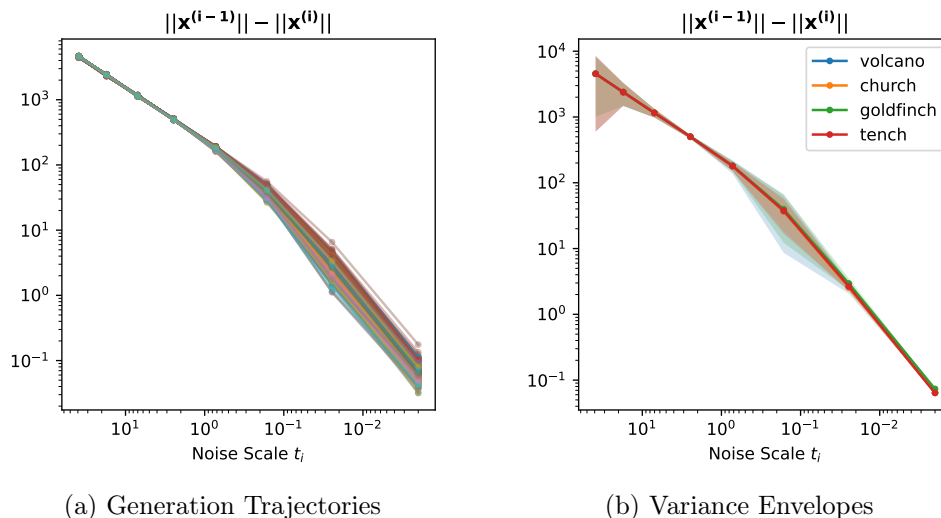


Figure 9: The difference in ℓ_2 norms of intermediate images between consecutive steps of the EDM sampling process. Figure (a) shows the evolution of $\|\mathbf{x}^{(i-1)}\| - \|\mathbf{x}^{(i)}\|$ (where i denotes sampling step) versus noise scale for 400 generation trajectories across 4 classes and (b) shows the mean with *variance* envelopes of the trajectories, aggregated by class. The sampling process clearly appears to be a contraction, supporting Empirical Observation 1



Figure 10: More samples from our diffusion-generated dataset, demonstrating the visual fidelity of the generated images. All 20 Imagenet64 classes used in our experiments are represented